Geophys. J. Int. (2004) **157,** 1393–1406 doi: 10.1111/j.1365-246X.2004.02313.x

Role of lateral mantle flow in the evolution of subduction systems: insights from laboratory experiments

Francesca Funiciello,[1,2] Claudio Faccenna[2] and Domenico Giardini[1]

[1] *Institute of Geophysics, ETH-Honggerberg, Zurich, Switzerland. E-mail: ffunicie@uniroma3.it*
[2] *Dipartimento di Scienze Geologiche, Università degli Studi 'Roma TRE', Roma, Italy*

Accepted 2004 March 5. Received 2004 January 19; in original form 2003 March 5

SUMMARY

We present 3-D laboratory experiments constructed to investigate the pattern of mantle flow around a subducting slab under different boundary conditions. In particular we present a set of experiments, characterized by different conditions imposed at the trailing edge of the subducting plate (that is, plate fixed in the far field, plate detached in the far field, imposed plate motion). Experiments have been performed using a silicone slab floating inside a honey tank to simulate a thin viscous lithosphere subducting in a viscous mantle. For each set, we show differences between models that do or do not include the possibility of out-of-plane lateral flow in the mantle by varying the lateral boundary conditions. Our results illustrate how a subducting slab vertically confined over a 660-km equivalent depth can be influenced in its geometry and in its kinematics by the presence or absence of possible lateral pathways. On the basis of these results we show implications for natural subduction systems and we highlight the importance of suitable simulations of lateral viscosity variations to obtain a realistic simulation of the history of subduction.

Key words: laboratory models, mantle flow, subduction.

1 INTRODUCTION

Slabs are complex 3-D entities. The most evident proof is shown by the strong variability of their lateral extension. In the earth system, in fact, the length of slabs varies over an order of magnitudes. Some slabs are very narrow (the Scotia, the Caribbean, the Cascades, the Banda, the Tyrrhenian and the Aegean slabs), while others are very long extending for thousand of kilometers (the Andean and the Mariana-Izu Bonin-Japan-Kurile-Kamchatka slab, see e.g. Jarrard 1986). The very irregular shape of a single Benioff zone represents additional evidence of the 3-D character of the subduction process. A slab changes dip angle, strike and state of stress along its length allowing the formation of arc and cusp geometries (Isacks & Barazangi 1977). A striking example of this feature is represented by the Chilean–Peru system, where flat portions of the slab border the steeper portion recognized below the Bolivian orocline (Cahill & Isacks 1992). Moreover, the geometry of the Wadati-Benioff isobaths shows without doubt that the slab deforms laterally. The analysis of the moment tensor solution for deep earthquakes of the Tonga slab reveals the presence of a systematic shear deformation superimposed on the mode of down-dip deformation, which is characteristic of the whole subduction zone (Giardini & Woodhouse 1984). This unique data set shows that mass of material within the slab can flow also along its strike in response to the interaction with a horizontal shear flow in the mantle. A similar inference has been also obtained by recent shear waves anisotropy studies and confirmed by laboratory models highlighting the role of the lateral escape of mantle material in retreating trench systems (Russo & Silver 1994; Buttles & Olson 1998).

Most of these observations have been interpreted on the basis of analogue and numerical geodynamic models bearing a fundamental 2-D geometry (Christensen & Yuen 1984; Kincaid & Olson 1987; Griffiths & Turner 1988; Gurnis & Hager 1988; Davies 1995; Griffiths *et al.* 1995; Guillou–Frottier *et al.* 1995; Zhong & Gurnis 1995; Houseman & Gubbins 1997; Olbertz *et al.* 1997), thus ignoring the above described 3-D geometry and mantle flow–slab interaction. Numerical approaches to 3-D subduction are still not producing satisfactory results for long-term subduction. Although an initially 3-D geometry can be maintained in models with purely viscous downwelling (Zhong *et al.* 1998), the long-term structure still resumes unrealistic two-sided symmetrical subduction (Tackley 2000a,b). Laboratory experiments are naturally 3-D. However, a true spherical setup has only been used in simple experiments used to reproduce the shape of subduction zones without slab–mantle interaction (Yamaoka *et al.* 1986). Nevertheless, experiments that include the mantle are formulated to suppress such 3-D aspects. The models are confined to 2-D by using a laterally homogenous slab structure controlled by the laterally confined box boundaries (Kincaid & Olson 1987; Shemenda 1992), or by using 2-D feeding pipes to inject the slab into a fluid of lower viscosity (Griffiths & Turner 1988; Griffiths *et al.* 1995; Guillou–Frottier *et al.* 1995).

In a previous paper (Funiciello *et al.* 2003) we have presented the first laboratory setup that includes a feedback of mantle flow and slab dynamics as constrained by 3-D boundary conditions. These experiments have analysed the dynamics of retreating slabs showing the key role of the lateral boundary conditions in controlling the behaviour of the subduction. We have found that the difference between models where lateral mantle circulation is permitted (laterally unconstrained models) or inhibited by lateral box boundaries (laterally constrained models) is particularly evident when the slab encounters a deep barrier representative of the 660-km discontinuity and the natural downflow component of mantle material is halted. This volumetric constraint generates a strong overpressure in the sub-mantle material that is high enough to slow down the slab retrograde motion. From this moment, the retreat of the slab can be achieved only by the lateral escape of sub-mantle material from the sides of the slab. When the mantle is allowed to escape along-strike away from the retreating slab in an unconstrained way, the effect of mantle overpressure is minimal. However, if the along-strike flow components are stopped by laterally constrained boundaries, the slab–mantle feedback influences the dynamics of subduction. Finally, we have argued that any lateral mantle outflow can strongly influence modelling results, restricting their possible application to natural systems.

Here we expand the analysis to a more general case of subduction where all possible motions of the incoming plate are considered. In fact, in Funiciello *et al.* (2003) we have chosen a reference frame fixed to the box (analogue of the hotspot reference frame) and we attached the trailing edge of the subducted plate in the far field to this reference. This ensured a system purely driven by the physics of trench retreat. Here, we use the same reference frame but we allow the incoming plate to be also detached or driven by a stepping motor.

2 MODEL SETUP

2.1 Model definition

We setup our experiments under the following framework.

2.1.1 Viscous rheology

The still rather elusive knowledge of the slab/lithosphere rheology (Karato *et al.* 2001) does not allow to constrain univocally this variable of the subduction simulations. In this work we follow the experimental choice adopted by previous authors (Kincaid & Olson 1987; Griffiths & Turner 1988; Griffiths *et al.* 1995; Guillou–Frottier *et al.* 1995; Faccenna *et al.* 1996; Becker *et al.* 1999; Faccenna *et al.* 1999) and we model the slab as an isoviscous body. The concept at the basis of this experimental approach is that the lithosphere in first approximation behaves like a viscous fluid in a process characterized by large temporal and spatial scale, such as subduction (Tao & O'Connell 1993).

We further simplify the slab rheology using a Newtonian fluid, whereas laboratory data indicates that upper-mantle materials should obey a creep power law of deformation (Brace & Kohlstedt 1980). As a Newtonian material has a stronger response to deformations than a power-law fluid (Ranalli 1995), the velocities observed in the laboratory should be considered as a lower bound.

2.1.2 Passive mantle

For the aim of this work, we are interested in the isolation of the mantle circulation produced by the subducting slab. Hence, we assume that the mantle is convectively neutral so that the only moment within it is that caused by the plate/slab system.

2.1.3 Reference frame

The reference frame of these experiments is the box boundary. It can be considered as the experimental analogue of the fixed hotspot reference frame.

2.1.4 Isothermal system

We are forced by laboratory limitations to neglect thermal effects during the subduction process. This implies that the model represents an end member essentially governed by the negative buoyancy of the slab (F_{sp}, Fig. 1). Temperature is translated into chemical density contrast, staying constant throughout the experiment. In this view, the slab is thought to be in a quasi-adiabatic condition. The high velocity of subduction (>1 cm yr^{-1}) recorded in our experiments justifies this assumption ensuring that we are representing a natural subduction system where conduction is limited (Peclet number$_{\text{equivalent Earth system}} \gg 1$; Turcotte & Schubert 1982)

The isothermal system implies also the impossibility of considering the fundamental role of phase changes in slab dynamics (Christensen & Yuen 1984; Pysklywec & Mitrovica 1998). In particular, we simulate the impediment of the slab to penetrate directly into the lower mantle only by the increase of viscosity with depth. This approximation is in agreement with the results of previous simulations where the effect of a viscosity increase with depth overcomes the one exerted by phase transformations (Bunge *et al.* 1997; Lithgow–Bertelloni & Richards 1998).

2.1.5 Impermeable lower mantle

We simulate the 660-km discontinuity as an impermeable barrier. The validity of this assumption is confirmed by previous studies, which found that the direct penetration of the slab through the transition zone is inhibited if the viscosity increase in the lower mantle is at least of an order of magnitude and if the timescale of the analysed process is limited (order of a few tens of million years) (Davies 1995; Guillou–Frottier *et al.* 1995; Christensen 1996; Funiciello *et al.* 2003). The first condition characterizes the Earth system where an increase in viscosity across this discontinuity by a factor of 10–100 has been postulated on the basis of models of wavelength of the geoid (Hager 1984; Hager & Richards 1989; King & Hager 1994) and postglacial rebound (Forte & Mitrovica 1996; Mitrovica & Forte 1997). The second condition is guaranteed in our experiments where we analyse only the short-term evolution of the subduction process (<50 Myr).

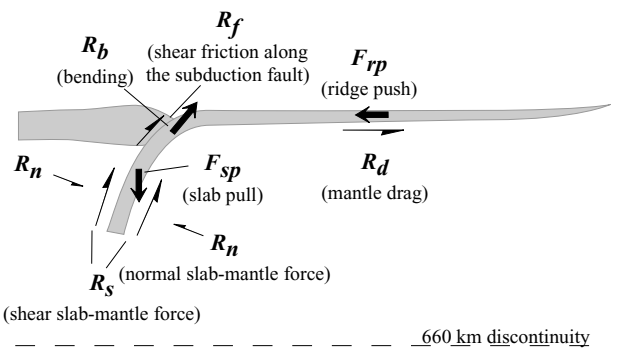

Figure 1. Forces at work in the subduction factory.

2.1.6 *Lack of the overriding plate*

In order to keep the setup as simple as possible, the overriding plate is not modelled. Hence we assume that:

(i) The effective viscosity of the weak zone (fault) is comparable with the upper-mantle viscosity. This choice is able to influence the rate of the subduction process but not its general behaviour (King & Hager 1990).

(ii) The shear friction along this weak fault (R_f, Fig. 1) has a secondary role in the modelling force balance of a mature subduction process confirming what has already been suggested by Zhong & Gurnis (1994) and Tichelaar & Ruff (1993).

(iii) The velocity of the overriding plate is negligible in respect to the velocity of the trench. Therefore, the applicability field of our experimental results is limited to natural cases characterized by this specific condition (i.e. Eurasian plate).

2.1.7 *Forces at work*

Although our models are simplified representations of the subduction, they have to be built to reproduce all the main forces of this natural process (Fig. 1). These forces can be presented as driving and resisting forces.

Following previous seminal papers (Forsyth & Uyeda 1975; Chapple & Tullis 1977; McKenzie 1977; Davies 1980; Conrad & Hager 1999; Funiciello *et al.* 2003), we identify in the slab pull (F_{sp}) and in the ridge push (F_{rp}) the driving forces of the subduction. In the experimental setup the body force, F_{sp}, is implemented by imposing a lithosphere denser than the underlying mantle. As discussed before, the initial constant density is assumed to be preserved during the whole subduction process. The horizontal compressional stresses originated from the cooling oceanic lithosphere, F_{rp}, are simulated using a rigid piston displaced at a constant horizontal rate to the plate margin.

The foremost resisting forces of the subduction process are the force necessary to bend the plate at the trench (R_b), the mantle drag force acting on the bottom of the subducting plate (R_d) and the slab–mantle interface forces (R_s, R_n) (Forsyth & Uyeda 1975; Chapple & Tullis 1977; McKenzie 1977; Davies 1980; Conrad & Hager 1999; Funiciello *et al.* 2003). The slab bending force can be expressed developing the theory for the bending of a viscous plate (Turcotte & Schubert 1982). Hence, we assume that the elastic deformation over long timescales can be incorporated in the viscous theory (England & McKenzie 1982). The order of magnitude of the viscous bending force is:

$$R_b \approx \frac{u h^3 \eta_{lit} w}{r^3}, \tag{1}$$

where η_{lit}, h, w and r are the dynamic viscosity, the thickness, the length of the trench and the radius of curvature of the bending slab and u is the subduction velocity. The mantle drag, R_d, on a plate should be proportional to the length (l) and velocity (u) of the plate and, also, to the viscosity of the underlying mantle (η_{um}; Forsyth & Uyeda 1975). This term can be neglected when $R_d \ll R_b$. It occurs when l is less than 1 order of magnitude larger than w. This inference holds because the radius of curvature of the subducting lithosphere at the trench is approximately of the same order of the thickness of the lithosphere (Becker *et al.* 1999) and η_m is two orders of magnitude smaller than η_{lit} (Hager 1984; Davies & Richards 1992; Mitrovica & Forte 1997). Finally, the shear and normal slab–mantle interface forces, R_s and R_n, are the result of the viscous resistance exerted by the displaced mantle on the slab. Both of them can be expressed in terms of corner flow theory for a fixed dip (Turcotte & Schubert 1982; Dvorkin *et al.* 1993):

$$R_s,\ R_n = \eta_{um} u \boldsymbol{L}, \tag{2}$$

where η_{um} is the upper mantle viscosity, $\boldsymbol{L}$ is the length of the subducted lithosphere and u is the averaged subduction velocity.

2.2 Materials

Following previous approaches (Kincaid & Olson 1987; Griffiths & Turner 1988; Griffiths *et al.* 1995; Guillou–Frottier *et al.* 1995; Faccenna *et al.* 1996; Becker *et al.* 1999; Faccenna *et al.* 1999) we use a multilayered setup. We select visco-elastic silicone putty (Rhodrosil Gomme, PBDMS + iron fillers) and Newtonian pure honey as an analogue of the lithosphere–upper-mantle system (Fig. 2).

Silicone putty is a visco-elastic material but the elastic component is negligible for the applied experimental strain rate (Weijermars 1986). Hence, the silicone putty can be considered as a quasi-Newtonian fluid where stress increases linearly with strain rate (Weijermars 1986; Weijermars & Schmeling 1986). The upper mantle has been modelled by honey, which is a Newtonian low-viscosity and high-density fluid (Table 1). These materials have been selected to simplify the stratified temperature-dependent Earth rheological profile respecting the standard scaling procedure for stress scaled down for length, density and viscosity in a natural gravity field ($g_{model} = g_{nature}$) as described by Weijermars & Schmeling (1986) and Davy & Cobbold (1991).

Viscosity and density are taken constant over depth of the individual layers, considering them as an average of effective values. The viscosity ratio of the oceanic lithosphere (η_{lit}) over the upper mantle (η_{um}) is fixed to 400 to ensure a realistic viscous coupling (Hager 1984; Davies & Richards 1992; Mitrovica & Forte 1997). The density contrast between the oceanic lithosphere and the upper mantle is set to 100 kg m^{-3} (Molnar & Gray 1979; Cloos 1993).

Materials parameters and the scaling relationships of a reference experiment are listed in Table 1. From the simple scaling equations we find that 1 min and 1 cm in the experiment correspond to 1 Myr and 60 km in nature, respectively.

2.3 Experimental procedure

The two-layer system is assembled in a rectangular Plexiglas tank (34-cm high, 58-cm long and 30-cm wide; Fig. 2). All the experiments are performed with an upper mantle scaled to have a thickness corresponding to 660 km.

We analyse two families of experiments, one in which the lateral mantle flow components are inhibited by lateral box boundaries and the other where they are permitted. We find that a laterally unconstrained system can be achieved by imposing, simultaneously (Fig. 2d):

(i) the plate width (w) lower than or equal to the thickness of the mantle circulation layer (H);

(ii) a distance between the plate/slab and box sides [$(b - w)/2$] greater than the size of the circulation cell, which in first approximation scales with the thickness of the mantle circulation layer (H).

In particular in the laterally constrained setup, the lateral effect of friction between plate slab and box is reduced by lubricating lateral walls with Vaseline.

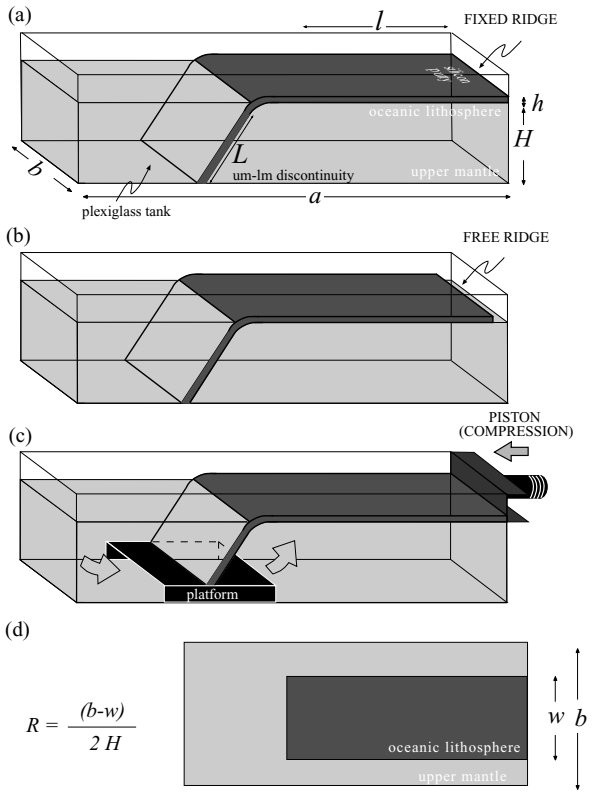

Figure 2. Sketch of the experimental setup. We show the three different boundary conditions adopted. (a) Experiments A1 and A2. The subducting plate is fixed to the box in the far field (fixed ridge *sensu* Kincaid & Olson 1987). This configuration simulates a system driven only by the negative buoyancy of the slab (F_{sp}) and resisted by the slab bending force (R_b) and the slab–mantle interface forces (R_s, R_n). (b) Experiments B1 and B2. The subducting plate is detached from the box boundary in the far field (free ridge *sensu* Kincaid & Olson 1987). This configuration is similar to the previous one but includes the effect of the mantle drag (R_d). (c) Experiments C1–C5. The trailing edge of the subducting plate is displaced with a rigid piston that pushes at constant horizontal velocity with reference to the box boundary. This simulates the case where subduction is essentially driven by plate motion. In experiments C3, C4 and C5 a rigid platform is added to the standard setup. This platform lies parallel to the bottom of the box from which it is approximately 8 cm distant. This configuration allows the mantle material that should escape from one side to return on the opposite side (periodic-like boundary condition). (d) Top view of the system. To express the lateral degree of freedom of the slab–mantle system, we identify the ratio R between half of the difference of the box width (b) and the plate width (w) and the thickness of the fluid (H). We analyse two families of experiments, one in which the lateral flow components are inhibited by lateral box boundaries ($R = 0$) and the other where they are permitted ($R = 1$).

In interpreting the results relative to the Earth, a laterally constrained setup may reproduce all the situations in which the work done by a mantle particle to move from the mantle wedge overlying the slab is minimized if achieved along down-dip directions (i.e. the inner portion of a wide subducting slab, a subduction system characterized by the presence of other nearby slabs). On the contrary, laterally unconstrained setup may be representative of natural systems in which 3-D subslab mantle flow develops preferentially trench-parallel mantle pathways (i.e. small slab).

Different boundary conditions are applied at the trailing edge of the subducting plate to explore a representative field of conditions occurring in the subduction system (Fig. 2):

(i) Fixed subducting plate (fixed ridge *sensu* Kincaid & Olson 1987; Fig. 2a). The slab-bearing plate is fixed to the box in the far field. This configuration simulates a system driven only by the negative buoyancy of the slab (F_{sp}) and resisted by the slab bending force (R_b) and the slab–mantle interface forces (R_s, R_n). We have analysed this case with application to subduction zones that belong to stable plates (i.e. Africa) and/or that have a lateral extension, at least, 10 times greater than the width of the slab-bearing plate.

(ii) Free subducting plate (free ridge *sensu* Kincaid & Olson 1987; Fig. 2b). The trailing edge of the subducting plate is detached from the box boundary. This configuration simulates a system driven by the slab pull (F_{sp}) and resisted by the slab bending forces (R_b), the mantle drag (R_d) and the slab–mantle interface forces (R_s, R_n). This simulates natural cases that occur in subduction zones where the width of the subducting plate is, at least, 10 times greater than the length of the trench (i.e. Western Pacific subduction zone).

(iii) Imposed plate motion (Fig. 2c). The trailing edge of the lithospheric plate is displaced with a rigid piston that pushes at a constant horizontal velocity with reference to the box boundary. This push adds to the forces presented in case (ii) and mimics the horizontal tectonic stresses resulting from the combined effect of ridge push (F_r) and plate re-organization. This case simulates a subduction essentially controlled by high rates of convergence of the incoming plate (i.e. Himalaya).

Experiments are performed analyzing the behaviour of these three different systems both with laterally constrained and unconstrained systems (Fig. 2d).

In the initial configuration, the leading edge of the silicone plate is forced downwards to a depth of 3 cm (corresponding to approximately 200 km in nature) inside the pure honey as a means to start the subduction process. Problems linked to the initiation of subduction (McKenzie 1977; Mueller & Phillips 1991; Ericksson & Arkani–Hamed 1993; Faccenna *et al.* 1999; Regenauer–Lieb *et al.* 2001) are beyond the scope of this paper. Experiments are executed at least twice to ensure reproducibility. Each experiment is monitored with a sequence of photographs taken in regular time in lateral and top views. We analysed the temporal changes in the trench motion, plate motion and intermediate dip of the slab (slab tangent at mid-mantle depth). Mantle streamlines on the surface are depicted by motion of inert tracers.

3 EXPERIMENTAL RESULTS

We perform 30 experiments to simulate the subduction of the oceanic lithosphere in a stratified mantle under a wide range of boundary conditions and using both laterally constrained and laterally unconstrained configurations. Here we describe the most representative experiments (Table 2) collected in three distinct classes.

3.1 Plate fixed in the far field

In this set of experiments the trailing edge of the subducting plate is fixed to the box. As a consequence, the movement of the plate is inhibited and the mantle drag force, R_d, is inactive.

Experiment A1 (Figs 3a and c, Table 2) is laterally constrained. The behaviour of the system during the free sink of the lithosphere into a stratified mantle is similar to what has been already

Table 1. Scaling of parameters in nature and in the laboratory for a reference experiment.

	Parameter		Nature	Reference model
g	Gravitational acceleration	m s^{-2}	9.81	9.81
	Thickness			
h	Oceanic lithosphere	m	70000	0.012
H	Upper mantle		660000	0.11
	Scale factor for length		$L_{\rm model}/L_{\rm nature} = 1.6 \times 10^{-7}$	
	Density			
$\rho_{\rm lit}$	Oceanic lithosphere	kg m^{-3}	3300	1482
$\rho_{\rm um}$	Upper mantle		3220	1383
	Density contrast ($\rho_l - \rho_{\rm um}$)		*80*	*99*
	Density ratio ($\rho_l/\rho_{\rm um}$)		*1.025*	*1.072*
	Viscosity			
$\eta_{\rm lit}$	Oceanic lithosphere	Pa s	10^{23}	1.6×10^5
$\eta_{\rm um}$	Upper mantle		10^{21}	40–400
	Viscosity ratio ($\eta_l/\eta_{\rm um}$)		10^2	4×10^{-2}–4×10^{-3}
	Characteristic time			
t	$(t_{\rm nature}/t_{\rm model} = (\eta_n/\eta_m)/(\sigma_n/\sigma_m) = (\eta_n/\eta_m)/((\Delta\rho\, gl)_n/(\Delta\rho\, gl)_m)$	s	3×10^{13} (1 Myr)	60 (1 min)

Table 2. Description of materials and parameters used in the selected experiments.

	$\rho_{\rm lit}$ (kg m^{-3})	$\rho_{\rm um}$ (kg m^{-3})	$\eta_{\rm lit}$ (Pa s)	$\eta_{\rm um}$ (Pa s)	$\eta_{\rm lit}/\eta_{\rm um}$	$\eta_{\rm um}/\eta_{\rm lm_{lm}}$	h (km)	H (cm)	R	Boundary conditions
A1	1482	1383	1.6×10^5	40–400	4×10^2–4×10^3	∞	1.2	11	0	Plate fixed
A2	1482	1383	1.6×10^5	40–400	4×10^2–4×10^3	∞	1.2	11	1	"
B1	1482	1383	1.6×10^5	40–400	4×10^2–4×10^3	∞	1.2	11	0	Plate detached
B2	1482	1383	1.6×10^5	40–400	4×10^2–4×10^3	∞	1.2	11	1	"
C1	1482	1383	1.6×10^5	40–400	4×10^2–4×10^3	∞	1.2	11	0	Plate forced
C2	1482	1383	1.6×10^5	40–400	4×10^2–4×10^3	∞	1.2	11	1	"
C3	1484	1383	1.6×10^5	40–400	4×10^2–4×10^3	∞	1.2	11	0	Forced motion, periodic-like boundary condition
C4	1484	1383	1.6×10^5	40–400	4×10^2–4×10^3	∞	1.2	11	1	"
C5	1484	1383	1.6×10^5	40–400	4×10^2–4×10^3	∞	1.2	11	1	Forced motion, periodic-like boundary condition, overriding plate

described in details in our previous experiments (Faccenna *et al.* 2001; Funiciello *et al.* 2003). During the first phase of the experiment, the trench retreats with a fast rate that increases progressively in time with the amount of subducted material. The dip of the slab also increases up to a maximum angle of 65°. Because the slab motion is retrograde, the process is always associated with a significant displacement of the mantle driven by the subducting lithosphere. Resulting streamlines are organized in two different cells above and beneath the subducting plate, respectively (Funiciello *et al.* 2003). Streamlines appear to be at a shallow angle to the slab in the vertical plane in accordance with the inference of Garfunkel *et al.* (1986).

A particular situation arises when the leading edge of the slab approaches the bottom boundary. At an equivalent depth of approximately 500 km, in fact, the slab already reduces its rate of retreat and its dip decreases by 10°. Simultaneously, a strong upper-mantle flow is forced to pass beneath the tip of the slab. Afterwards, the slab touches the bottom boundary and the trench retreat slows down for approximately 5 Myr. After the interaction, the trench starts to bend laterally into an arc shape allowing lateral circulation of mantle material around the slab and resuming the trench retreat. From this moment, the trench retreat velocity is approximately constant and the slab dip reaches steady-state values of approximately 50°, while the slab tip lies horizontally on top of the lower mantle.

In experiment A2 (Figs 3b and c, Table 2) only the width of the subducting plate is varied, allowing investigation of the behaviour of the same setup in a laterally unconstrained configuration. As in experiment A1, the subduction starts by increasing the rate of trench retreat and dip. The bottom of the upper mantle is reached rapidly (after 7 Myr) with a steeper dip (∼70°) than in the constrained case. The trend of subduction changes again when the slab interacts with the 660-km discontinuity. Subduction slows down while the tip of the slab folds and deforms at depth. The trench restarts to retreat after only 2 Myr and it preserves its initial linear shape during the entire duration of the experiment. Results of these two simple experiments illustrate the importance of lateral mantle flow components in the dynamics of subduction.

3.2 Plate detached in the far field

In this set of experiments, the trailing edge of the incoming plate is detached from the box. Hence, the plate is free to move and the mantle drag force at the base of the plate, $R_{\rm d}$, is active.

Experiment B1 (Figs 4a and c, Table 2) is laterally confined. The behaviour of the slab during the free fall into the mantle is the same as observed previously: the rate of trench retreat increases progressively in time with the amount of subducted

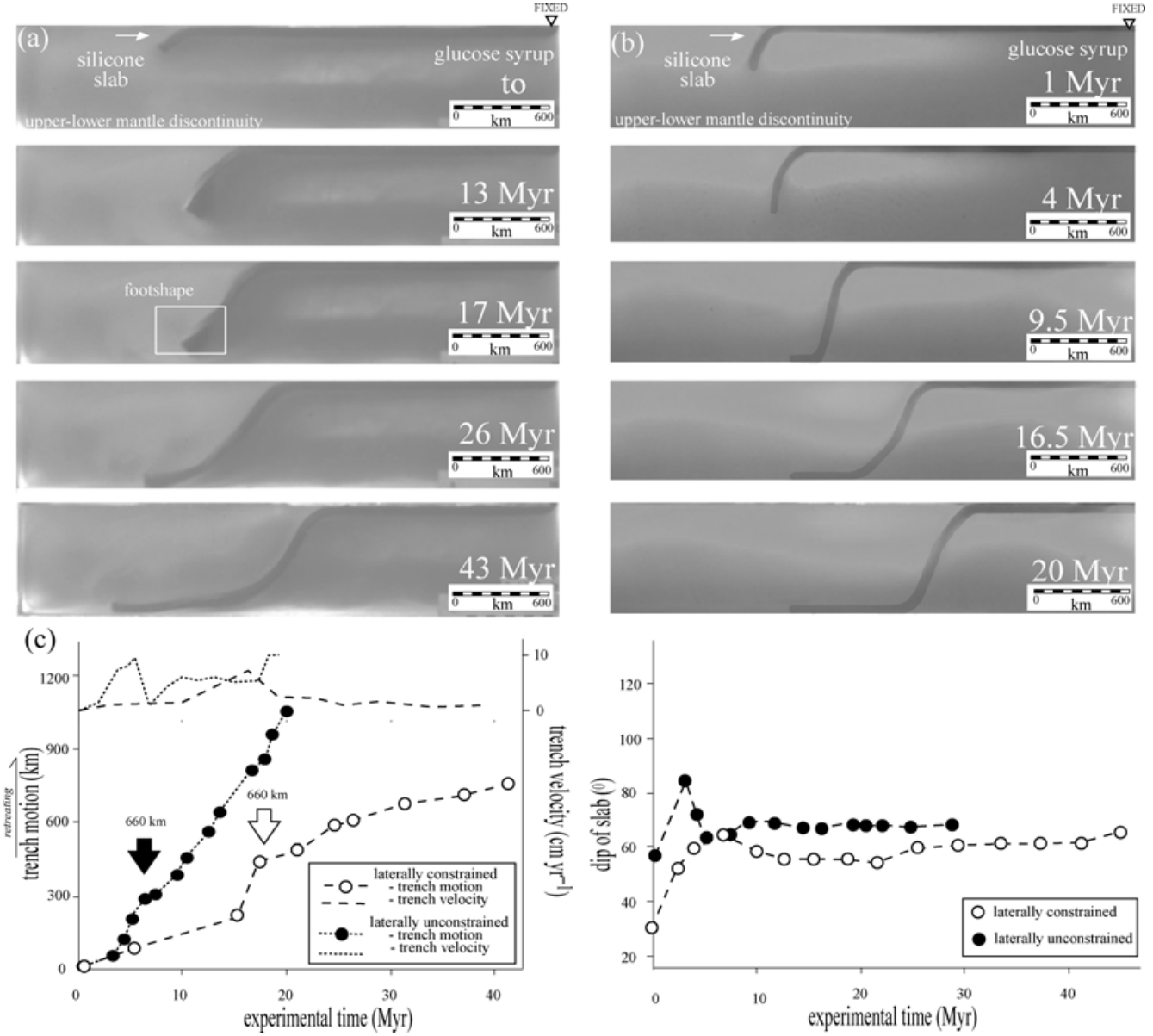

Figure 3. Stages of evolution of the experiments A1 (a) and A2 (b) characterized by a fixed trailing edge as boundary conditions and by laterally constrained and unconstrained setting, respectively. (c) Plot of the amount of trench retreat, velocity of trench retreat and dip vs. time for both the experiments. The arrow indicates the time of interaction with the 660-km discontinuity. The error bar on the measurements is of half a degree for angles and half a centimetre for length (equivalent to 30 km in nature), respectively.

material. At the same time, also the dip of the slab increases catching up to the maximum value of approximately 85°. The intensity of the induced mantle flow is less than observed for cases A. This condition arises from the motion of the incoming plate, which allows compensation for the retreating motion of the trench. As a consequence, less overpressure is created beneath the subducting plate. When the slab reaches the bottom box boundary the trench slows down and subsequently shows a prograde motion (Fig. 4c). After this interaction phase lasting approximately 10 Myr, the slab bends at depth and the trench starts moving again in a slow retreating mode. This phase can be described by a linear and smooth increase of trench retreat and by an increase of the dip that reaches values higher than 90° giving the slab an overturned shape.

Experiment B2 (Figs 4b and c, Table 2) is similar to the previous one but the plate/slab system is laterally unconstrained. During the fall into the upper mantle, the trench retreats with a constant velocity and the slab increases its dip to reach an overturned configuration. Once the slab reaches the 660-km discontinuity (after approximately 10 Myr), the tip of the slab folds at depth and, simultaneously, the trend of subduction changes to a forward migration. The trench advances considerably for approximately 20 Myr while the slab attains an open reclined U-shape. Afterwards, the open U closes as a result of hinge collapse and the dip of the slab stabilizes at approximately 60°. Subsequently, the trench starts to retreat again at a constant velocity. In both experiment B1 and B2 the trench keeps its initial linear shape at the surface.

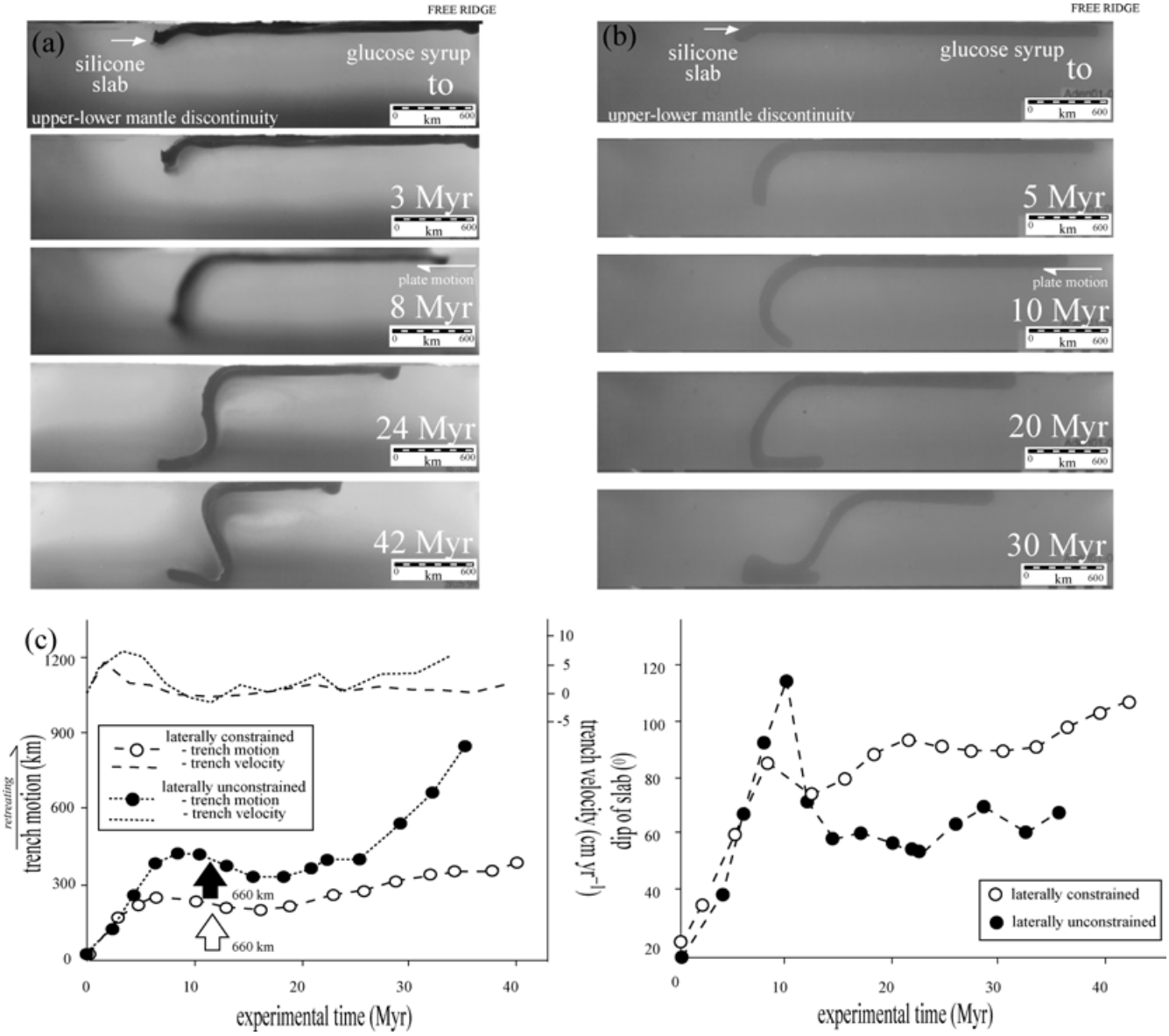

Figure 4. Lateral view of evolution of the experiments B1 (a) and B2 (b) characterized by a free trailing edge as boundary conditions and laterally constrained and unconstrained setting, respectively. (c) Plot of the amount of trench retreat, trench velocity and dip vs. time.

An interesting difference between the two models appears when the trend of plate motion is analysed (Fig. 5). The plate velocity of the laterally constrained case (experiment B1) is significantly larger than the velocity of the unconstrained case (experiment B2), especially after the interaction phase at 20 Myr. This is because the overpressure produced beneath the slab propels the plate at a faster rate during the overturning of the slab. This effect is smoothed out once the mantle overpressure behind the slab is decreased as a result of the possibility for the mantle to flow on the lateral sides of the plate/slab.

3.3 Imposed plate motion

In this set of experiments we study the effect of pushing the plate at a constant horizontal velocity against the subduction zone, by displacing a rigid piston on the trailing edge of the oceanic lithosphere.

In the first set of experiments, we add a horizontal convergence velocity of 1.5 cm min^{-1} (corresponding to approximately 10 cm yr^{-1} in nature, i.e. Western Pacific Plate). Once more, experiments laterally constrained and unconstrained (C1 and C2, respectively) differ. The behaviour of C1 (Figs 6a and c, Table 2) can be separated in two different domains, before and after the interaction with the transition zone, while the variations of the position of the trench are contained to only approximately 30 km. The position of the trench is characterized by an initial limited forward trend that becomes retrograde when the leading edge of the slab is close to the upper–lower mantle discontinuity. Trench migration stops when the slab interacts with the lower boundary. From this moment, the imposed plate velocity is distributed between the sliding of the slab on the bottom and buckling deformation of the lithosphere near the piston.

The geometric evolution of experiment C2 (Fig. 6b and c, Table 2) is quite similar to what has been already observed in C1.

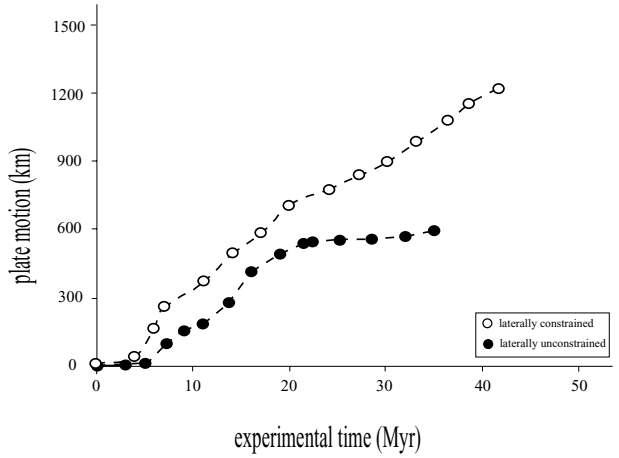

Figure 5. Plot plate motion vs. time of experiments B1 and B2, characterized by laterally constrained and laterally unconstrained configurations, respectively.

However, a significant difference appears in terms of kinematics, where a laterally constrained system like C1 leads to trench arrest while the laterally open case C2 allows an advancing trench after the interaction with the 660-km discontinuity.

Obviously, volumetric locking of the system controls these results. We observe that in the laterally constrained experiment C1, vertical mantle streamlines interact with box boundaries giving rise to strong anomalous overpressure and a lowing down of subduction owing to buckling deformation in front of the piston.

To verify if and how the volumetric locking plays the key role in these results, we perform a second set of experiments in which we introduce periodic-like boundary conditions for the mantle (Fig. 2c). This configuration can be obtained by adding a rigid platform to the standard setup. This platform lies parallel to the bottom of the box from which it is approximately 8 cm distant (see Fig. 2c).

Once more, we perform a series of experiments characterized by lateral constrained and unconstrained conditions, respectively. In both of them the advancing piston moves at an averaged velocity of 0.8 cm min^{-1} (corresponding to approximately 5 cm yr^{-1} in nature).

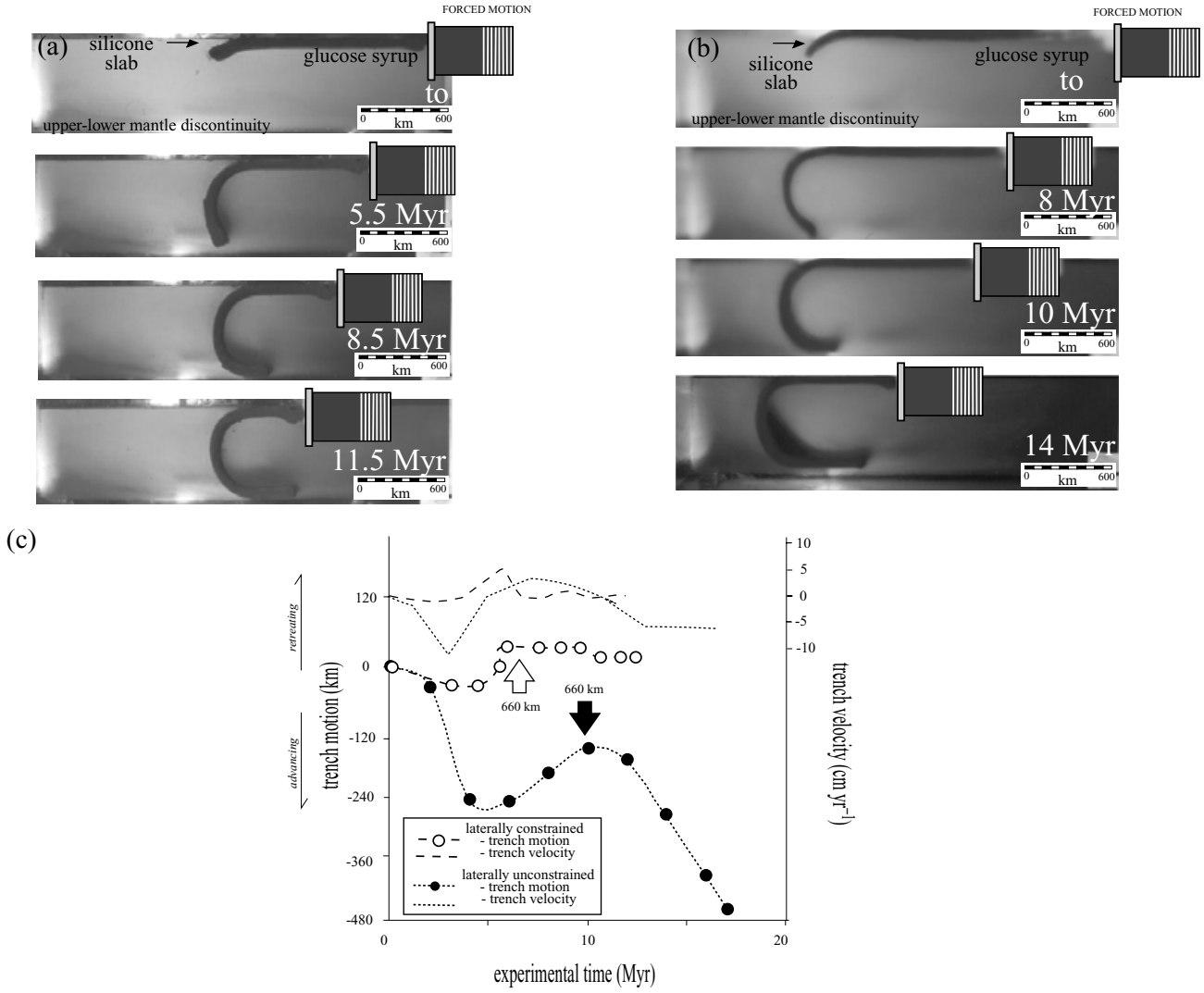

Figure 6. Lateral view of evolution of the experiments C1 (a) and C2 (b) characterized by an imposed horizontal velocity of convergence of 1.5 cm min^{-1} (corresponding to approximately 10 cm yr^{-1} in nature) and by laterally constrained and unconstrained configuration, respectively. (b) Plots showing the evolution in time of the trench retreat and trench velocity.

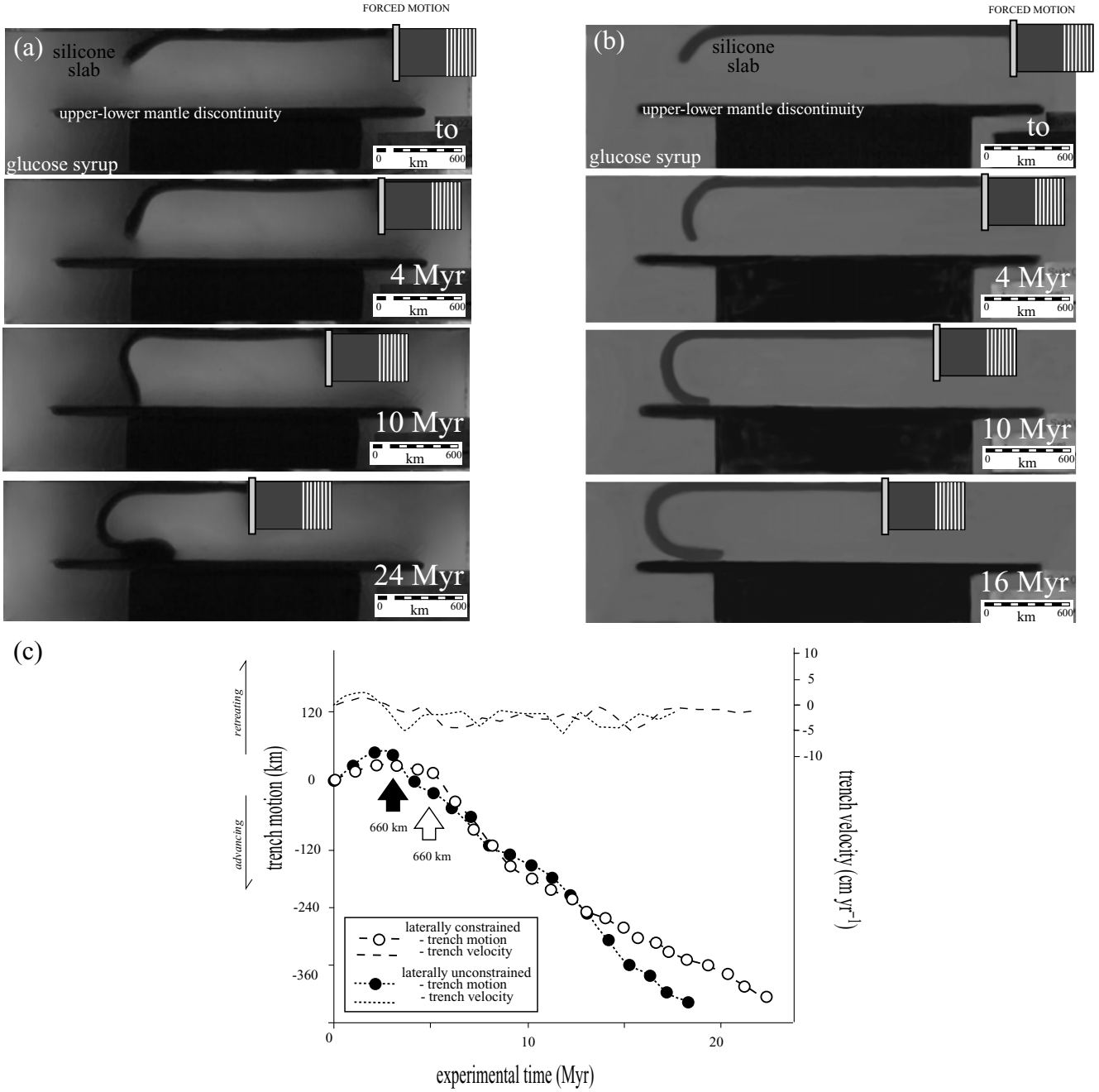

Figure 7. Lateral view of evolution of the experiments C3 (a) and C4 (b) characterized by an imposed horizontal velocity of convergence of 0.7 cm min^{-1} (corresponding to approximately 5 cm yr^{-1} in nature) and by laterally constrained and unconstrained configuration, respectively. (b) Plots showing the evolution in time of the trench retreat and trench velocity.

The behaviour of the laterally constrained experiment C3 (Figs 7a and c, Table 2) differs substantially from the one observed in C1 (the comparison has to take into account the changed velocity condition that varies the rate of the subduction process). The experiment shows a typical sequence of distinct phases. During the first phase, the slab falls into the upper mantle while, simultaneously, the trench retreats and the dip of the slab increases reaching a near vertical configuration. Once the slab reaches the 660-km discontinuity, it folds at depth. In this second phase, the trench motion slows down for a few Myr while the slab assumes a reclined shape. From this time, the third phase occurs during which the geometry of the system becomes invariable and the trench advances at a near-constant velocity.

On the contrary, the laterally unconstrained experiment, C4 (Fig. 7b and c, Table 2), does not differ from C2. Although the imposed horizontal convergence velocity of C4 is only half of the value adopted in C2, there appears to be a rule the presence of three phases, the first two characterized by a transient behaviour and the third of steady state. Summing up, the prograde motion of the trench after the interaction with the 660-km discontinuity and the consequent reclined shape is a rule of experiments performed with periodic-like boundary conditions.

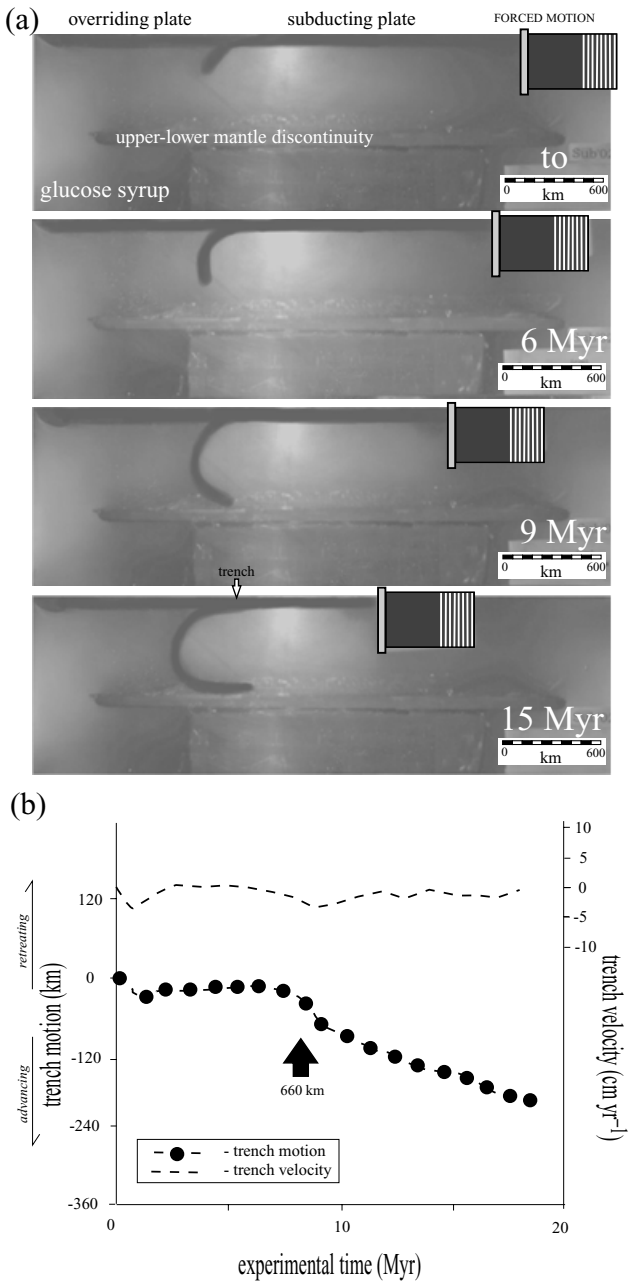

Figure 8. (a) Lateral view of four stages of evolution of the experiment C5 characterized by a forced trailing edge, a laterally unconstrained configuration and the presence of the overriding plate. (b) Plot showing the evolution in time of the trench retreat and trench velocity.

In order to confirm the general validity of our result, we test the possible influence of the presence of an overriding plate that is attached to our reference frame. In experiment C5 (Fig. 8, Table 2) a fixed plate with a lower mean bulk density than the honey is added to the system as an analogue of the overriding plate. As in experiments C3 and C4, the advancing piston moves at an averaged velocity of 0.8 cm min^{-1} (corresponding to approximately 5 cm yr^{-1} in nature). A 0.5-cm-wide lubricated Vaseline zone separates the two plates ensuring that the fault zone viscosity remains the one of the mantle. The slab behaviour is similar to the previous experiments. We note that the presence of the overriding plate affects only the timescale of our results and not the general style. An interesting aspect of this experiment is an underplating of the overriding plate corresponding to 200–300 km, which does not appear to affect the gross evolution of the process.

4 INTERPRETATION OF EXPERIMENTAL RESULTS AND DISCUSSION

We set up experiments in the laboratory to test the influence of the lateral boundary conditions on subduction dynamics, imposing three different conditions at the trailing edge of the plate/slab system to cover a wide range of geodynamic configurations: fixed, free or pushed with respect to the reference frame of the box.

Independently from the adopted boundaries conditions, we identify three distinct phases in the evolution of the subducting slab: (i) the sink of the slab into the upper mantle; (ii) the interaction with the 660-km discontinuity; (iii) the final phase of steady state with the slab that lies on the upper-/lower-mantle transition zone. These three different phases vary as a function of the boundary conditions imposed at the trailing edge of the subducting plate. Comparison between laterally constrained and unconstrained models also shows that the style of subduction can be largely modified by the possibility for the flow to turn around the slab. The lateral migration of the subducted plate produces a significant and geometrically complex mantle circulation. The moving plate, in fact, produces a non-hydrostatic pressure-drop in the two separate cells produced on the top and bottom of the slab by the slab–mantle viscous coupling. To re-balance the equilibrium of the system, mantle flows laterally from the high- to low-pressure area. Induced mantle flow has different characteristics before and after the slab reaches the bottom of the circulation system. In accordance with experimental results of Buttles & Olson (1998) and Funiciello *et al.* (2003), we find that the poloidal component prevails during the subduction into the upper mantle (stage 1). Mantle fluxes are preferentially oriented beneath the slab. The poloidal flow is inhibited when the slab starts to interact with the stiff impermeable bottom layer (stages 2–3). Dissipation of overpressure into the upper mantle is, therefore, only possible if the flow moves sideways assuming a prevalent toroidal component (Fig. 9, stage 3 of experiements A, B and C). This mass redistribution within the mantle creates an additional pressure in the system that should be included in the force equilibrium. In fact, our results show that rate of subduction and trench migration are slower if the lateral mantle flow is inhibited.

In particular, stage 1 is characterized by a progressive increase of the rate of trench retreat and of the dip of the slab. A different rate of trench retreat is a function of the adopted boundary conditions. A plate fixed in the far field (experiments A1 and A2) produces a fast trench retreat. A detached (experiments B1 and B2) or pushed (experiments C1 and C2) plate, results in a slower trench motion (particularly for experiments C1 and C2), as the amount of subduction is now partitioned between trench and plate motion. Of course, in the case of experiments C1 and C2, the imposed motion of the plate absorbs a larger portion of the subduction. During stage 1, we do not observe a remarkable difference between laterally constrained and unconstrained models, indicating that mantle material flows preferentially below the slab, attaining a poloidal component. During stage 2, the tip of the slab interacts with the 660-km discontinuity. In this stage we note a large difference between constrained and unconstrained models, showing the presence of an important out-of-plane component of mantle flow.

In the fixed plate experimental set (experiment A1; Figs 3a, c and 9), the overpressure produced by the retreating slab triggers a

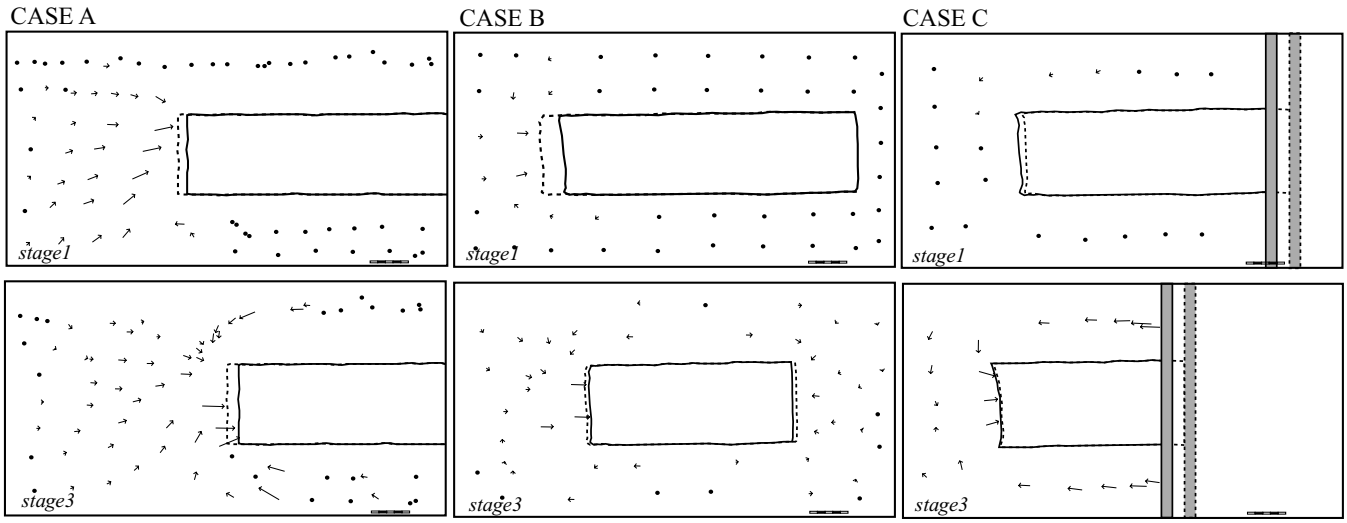

Figure 9. Line drawings of top view of experiments illustrating mantle circulation pattern in the mantle before (stage 1) and after (stage 3) the slab/660-km discontinuity interaction defined by means of the passive markers floating on the top surface. Experiment A2 (plate fixed in the far field; a) between t_0 and $t = 2$ min and (b) between $t = 10$ and $t = 12$ min. Experiment B2 (plate detached in the far field; c) between t_0 and $t = 2$ min and (d) between $t = 19$ and $t = 21$ min. Experiment C4 (imposed plate motion; e) between t_0 and $t = 2$ min and (f) between $t = 10$ and $t = 12$ min. Length of vectors indicates the amount of displacement, while the arrowhead indicates the direction of displacement. Dashed and full lines indicate the contours of the subducting plate at the beginning and at the end of the selected temporal window. The mantle flow shows different features before and after the slab reaches the upper-/lower-mantle boundary. The ubication and the direction of the vectors during stage 1 are interpreted as being the result of the prevalent poloidal component of the mantle flux during the subduction into the upper mantle (Funiciello *et al.* 2003). Conversely, the ubication and the direction of the vectors during stage 3 are interpreted as being the result of the prevalent toroidal component of the mantle flux after the interaction of the slab with the 660-km discontinuity.

flow in the mantle that is forced (as a result of the fact that the plate is fixed) to pass trough the closing channel between the lower tip of the slab and the bottom of the box (Fig. 3a; 17 Myr). The flow becomes overly strong and deforms the geometry of the tip of the slab, which assumes a typical foot shape. Once the channel is closed the system halts for the time necessary to deform the slab laterally, allowing the mantle to escape and to resume its circulation. Both the time of arrest and the amount of arcuation of the trench are proportional to the slab strength (Funiciello *et al.* 2003). Allowing lateral circulation (experiment A2; Figs 3b, c and 9), these effects are minimized and we note only a slow down of the system related to the deformation at depth of the slab tip and by the simultaneous dynamic re-equilibration of mantle pathways. Moreover, the straight shape of the trench is maintained. During stage 3, the model attained a similar behaviour as the plate is deformed enough to ensure the presence of lateral mantle flow.

When the plate is detached in the far field (experiments B1 and B2; Figs 4 and 9), overpressures produced in the mantle beneath the slab can be dissipated also by means of plate motion. In fact, the plate starts moving when the slab is close to the 660-km boundary. The largest amount of plate motion is recorded in the laterally constrained setting, where lateral flow is inhibited. Under this condition, it is energetically more suitable to generate a considerable drag of the plate rather than the lateral arcuation. The shape of the slab represents another intriguing difference between laterally constrained and unconstrained models. In the first category of models, in fact, mantle streamlines are still forced to pass trough the channel between the lower tip of the slab and the base of the circulating system supporting the steepening of the slab. On the contrary, the slab always assumes a reclined shape in laterally unconstrained models. After the interaction with the 660-km discontinuity, both models present a limited interval characterized by the advancing motion of the trench followed by a retreating trend. The rate of trench retreat during the last stage is sensible to the possibility for the flow to escape laterally from beneath the slab: the unconstrained setting shows a higher rate of trench retreat and a lower rate of plate motion. This derives from the fact that in an constrained setting the overpressure created beneath the slab is dissipated in the form of flow dragging the plate toward the subduction zone (Fig. 5). In the laterally unconstrained model, instead, the trench clearly advances during the transitional phase of re-equilibration of mantle fluxes while the slab tip is folded again for the third bending. The passage from a behaviour of trench advancing to a behaviour of trench retreating is controlled by the compatibility with the deep folding instability.

When imposed plate motion is applied to the system (experiments C1 and C2; Figs 6, 7, 8 and 9), the amount of trench motion during the fall into the upper mantle is limited and able to create only small pressure differences. The slab interacts with the discontinuity always assuming a reclined shape. At the moment of interaction, the double bending at depth governs the resistive force of the system. Additional energy is provided by the pushing piston, giving an essentially advancing trend of the trench. Owing to the controlling role of the piston, experiments C1 and C2 always resumes a steady state both in the laterally constrained and unconstrained models. The velocity in experiments C1 and C2 translates into slab velocity as a function of the lateral boundary conditions. The highest value is recorded in the laterally unconstrained model, where the displaced mantle can freely flow backwards and very little buckling deformation occurs adjacent to the piston. For the entirely closed experiment, C1, the lowest value is obtained as a result of significant partition between sliding and buckling deformation.

This common general behaviour is insensitive to the lack of the overriding plate. In agreement with King & Hager (1990), we find that higher resistance of subduction fault influences the timescale of the process but not the general character of its evolution (experiment C5; Fig. 8). Nevertheless, results produced by this category of models can be strongly affected by the volumetric locking of the

system. For example, the trench advance can be inhibited in a laterally constrained system that is not implemented with periodic-like boundary conditions able to easily dissipate eventually anomalous overpressures (i.e. experiment C1). The slab imposes an artificial volumetric locking between the two distinct upper-mantle circulation cells. In the impossibility of the slab being laterally bent because of the extreme rapid velocity of the process, strong anomalous mantle overpressures are produced at the top of the subduction plate. Their action resists the advancing motion of the trench producing a fake effect of a stationary trench and a progressive increase of the dip at the trench. These stationary conditions can sustain the direct penetration of the slab into the lower mantle. However, it is necessary to keep in mind that it is only an effect produced by the volumetric limitation.

Summarizing our results, we can say that the episodic behaviour of the slab during the subduction and interaction with the upper/lower mantle transition zone is controlled by forces active in the system whose distribution is influenced by the choice of adopted boundary conditions. Retreating motion of the trench emerges to be the general rule. Advancing motion of the oceanic plate is possible but only under specific conditions. We also highlight the significance and consequences of slab–mantle interactions. The lateral escape of mantle material produced by the migration of the subducting slab has an important role on the kinematics of subduction. The possibility to dissipate mantle overpressure produces a general increase in the rate of trench migration.

The models presented here have been designed to investigate the style of subduction and trench migration under different boundary conditions. We believe that our results have important consequences if compared with subduction models that have been performed under the assumption that material cannot flow laterally out-of-plane (2-D condition or 3-D laterally constrained setting). In the light of our results, the choice of the most appropriate model that can be applied to natural cases should be made considering the expected pathway of the mantle material. One can imagine that in the centre of a very wide and continuous subduction zone the approximation to a perfectly 2-D setting can hold on. However, this kind of approximation also has to take into account the fact that the rate of migration of mantle material scales with its viscosity. For the case of a narrow slab, conversely, we are forced to consider that material can easily escape out of the plane, facilitating the retreating process that proceeds at a faster rate. We can evaluate the critical length able to differentiate laterally constrained and unconstrained subduction zone by means of a simple calculations. Assuming that the trench-parallel mantle flow is equivalent to a simple channel flow (Turcotte & Schubert 1982), it is possible to express the averaged flow velocity, u, as:

$$u = -\frac{l^2}{12\eta}\frac{dp}{dx}, \tag{3}$$

where η is the viscosity, l is the thickness of the channel and dp/dx is the pressure gradient. We further assume that dp/dx is related to the slab pull force, $dp/dx = \Delta\rho g h/D$, where $\Delta\rho$ is the density contrast between the lithosphere and the underlying mantle, g is the gravitational acceleration, h is the thickness of the subducting lithosphere and D is the half-length of the trench. Assuming $\eta = 10^{21}$ Pa s, $\Delta\rho = 80$ kg m^{-3}, $h = 70$ km and l the thickness of the upper mantle (660 km), we can estimate that even a 10 000-km width subduction slab should be considered as a laterally open structure, as on its sides it would be affected by a mantle flow at rate of approximately 1 cm yr^{-1}. In other words, it is possible that the trend and evolution of subducting slabs are strongly influenced by lateral motion of subslab mantle material. Hence, their evolution should be simulated using a 3-D setting.

Our results also confirm previous findings that slabs preferentially show a retreating motion (Chase 1978; Uyeda & Kanamori 1979; Dewey 1980; Garfunkel *et al.* 1986; Richards & Engebreston 1992). Advancing trenches are only limited to cases where the mantle can easily flow laterally and the subducting plate is governed by the energy supplied by plate motion. However, we find that none of our single-slab experiments are suited to simulating appropriately the Pacific case, where the subducting plate is moving forward and trenches are rolling back. A possible explanation of this behaviour can be related to the particular plate-jigsaw-like geometry of plates in the Pacific. There are numerous slabs that show a wide variety of deformation styles at the transition zone. Hence, we can argue that the subduction velocity is controlled by the ensemble of slabs and cannot be described by a single-slab model. Other possible improvements for future laboratory modelling of slabs are increasing the elastic strength of slabs and varying laterally viscosity and density to mimic natural settings. Because our experiments give an appropriate account of magnitudes of driving and resisting forces, the central conclusions concerning the physics of subduction should, however, be considered valid.

5 CONCLUSIONS

We describe laboratory experiments that investigate the kinematics of a slab falling into the mantle in laterally constrained and unconstrained systems. We find that the plate/slab system has a highly dynamic equilibrium during the fall into the upper mantle and the interaction with the 660-km transition zone with distinct characteristic phases of behaviour. The character of these phases is governed by forces active in the system whose distribution is influenced by the choice of adopted boundary conditions. Our results show that a strong contribution is offered by the effect of slab–mantle interactions. The lateral slab migration, in fact, generates a complex 3-D flux in the mantle characterized by a time dependent behaviour. This additional component cannot be ignored and its importance is fundamental when the slab reaches the limit of the circulation system. Our results illustrate how a subducting slab can be influenced not only in its shape but also its kinematics through the presence or absence of possible lateral pathways where the mantle can escape. On the basis of these results, we highlight the importance of a suitable simulation of lateral viscosity variation to obtain realistic simulation of the history of subduction.

ACKNOWLEDGMENTS

Experiments have been performed in the Laboratory of Experimental Tectonics of the University of 'Roma TRE'. Discussions with Klaus Regenauer–Lieb, Gabriele Morra and Nicolas Bellahsen improved the quality of the work. Special thanks to Klaus Regenauer–Lieb for reviewing several versions of the paper. The paper benefited from the constructive reviews of Yanick Ricard, Joseph Martinod and Laurent Guillou–Frottier. This is publication 1322 of the Institute of Geophysics, ETH Zürich.

REFERENCES

Becker, T.W., Faccenna, C., O'Connell, R.J. & Giardini, D., 1999. The development of slabs in the upper mantle: Insights from numerical and laboratory experiments, *J. geophys. Res. – Solid Earth,* **104,** 15 207–15 226.

Brace, F.W. & Kohlstedt, D.L., 1980. Limits on lithospheric stress imposed by laboratory experiments, *J. geophys. Res.,* **50,** 6248–6252.

Bunge, H.P., Richards, M.A., Engebretson, D.C. & Baumgardner, J.R., 1997. A sensitivity study of three-dimensional spherical mantle convection at 108 Rayleigh number: effects of depth-dependent viscosity, heating mode and endothermic phase change, *J. geophys. Res.,* **102,** 11 991–12 007.

Buttles, J. & Olson, P., 1998. A laboratory model of subduction zone anisotropy, *Earth planet. Sci. Lett.,* **164,** 245–262.

Cahill, T. & Isacks, B.L., 1992. Seismicity and shape of the subducted Nazca plate, *J. geophys. Res.,* **97,** 17 503–17 529.

Chapple, W.M. & Tullis, T.E., 1977. Evaluation of the forces that drive the plates, *J. geophys. Res.,* **82,** 1967–1984.

Chase, C.G., 1978. Plate kinematics: the Americas, East Africa and the rest of the world, *Earth planet. Sci. Lett.,* **37,** 357–368.

Christensen, U.R. & Yuen, D., 1984. The interaction of the subducting lithospheric slab with a chemical or phase boundary, *J. geophys. Res.,* **89,** 4389–4402.

Christensen, U.R., 1996. The influence of trench migration on slab penetration into the lower mantle, *Earth planet. Sci. Lett.,* **140,** 27–39.

Cloos, M., 1993. Lithospheric Buoyancy and Collisional Orogenesis - Subduction of Oceanic Plateaus, Continental Margins, Island Arcs, Spreading Ridges, and Seamounts, *Bull. geol. Soc. Am.,* **105,** 715–737.

Conrad, C.P. & Hager, B.H., 1999. Effects of plate bending and fault strength at subduction zones on plate dynamics, *J. geophys. Res.,* **104,** 17 551–17 571.

Davies, G.F., 1980. Mechanics of subducted lithosphere, *J. geophys. Res.,* **85,** 6304–6318.

Davies, G.F. & Richards, G.F., 1992. Mantle convection, *J. Geol.,* **100,** 151–206.

Davies, G.F., 1995. Penetration of plates and plumes through the mantle transition zone, *Earth planet. Sci. Lett.,* **133,** 507–516.

Davy, P. & Cobbold, P.R., 1991. Experiments on shortening of a 4-layer continental Lithosphere, *Tectonophysics,* **188,** 1–25.

Dewey, J.F., 1980. Episodicity, sequence and style at convergent plate boundaries, in *The continental crust and its mineral deposits*, pp. 553–573, ed. Strangway, D.W., Geological Association of Canada Special Paper 20.

Dvorkin, J., Nur, A., Mavko, G. & Ben, A.Z., 1993. Narrow subducting slabs and the origin of backarc basins, *Tectonophysics,* **227,** 63–79.

England, P. & McKenzie, D., 1982. A thin viscous sheet model for continental deformation, *Geophys. J. R. astr. Soc.,* **70,** 295–321.

Ericksson, S.G. & Arkani–Hamed, J., 1993. Subduction initiation at passive margins: the Scotian Basin, Eastern Canada as a potential example, *Tectonics,* **12,** 678–687.

Faccenna, C., Davy, P., Brun, J.P., Funiciello, R., Giardini, D., Mattei, M. & Nalpas, T., 1996. The dynamic of backarc basins: an experimental approach to the opening of the Tyrrhenian Sea, *Geophys. J. Int.,* **126,** 781–795.

Faccenna, C., Giardini, D., Davy, P. & Argentieri, A., 1999. Initiation of subduction at Atlantic-type margins: insights from laboratory experiments, *J. geophys. Res.,* **104,** 2749–2766.

Faccenna, C., Funiciello, F., Giardini, D. & Lucente, P., 2001. Episodic back-arc extension during restricted mantle convection in the Central Mediterranean, *Earth planet. Sci. Lett.,* **187**(1–2), 105–116.

Forsyth, D. & Uyeda, S., 1975. On the relative importance of the driving forces of plate motion, *Geophys. J. R. astr. Soc.,* **43,** 163–200.

Forte, A.M. & Mitrovica J.X., 1996. New inferences of mantle viscosity from joint inversion of long-wavelength mantle convection and post glacial rebound data, *Geophys. Res. Lett.,* **23,** 1147–1150.

Funiciello, F., Faccenna, C., Giardini, D. & Regenauer–Lieb, K., 2003. Dynamics of retreating slabs (part 2): insights from 3-D laboratory experiments, *J. geophys. Res.,* **108**(B4), 10.1029/2001JB000896.

Garfunkel, Z., Anderson, D.L. & Schubert, G., 1986. Mantle circulation and lateral migration of subducting slabs, *J. geophys. Res.,* **91,** 7205–7223.

Giardini, D. & Woodhouse, J.H., 1984. Deep seismicity and modes of deformation in Tonga subduction zone, *Nature,* **307,** 505–509.

Griffiths, R.W. & Turner, J.S., 1988. Folding of viscous plumes impinging on a density or viscosity interface, *Geophys. J.,* **95,** 397–419.

Griffiths, R.W., Hackney, R.I. & Vanderhilst, R.D., 1995. A Laboratory Investigation of Effects of Trench Migration on the Descent of Subducted Slabs, *Earth planet. Sci. Lett.,* **133,** 1–17.

Guillou–Frottier, L., Buttles, J. & Olson, P., 1995. Laboratory experiments on structure of subducted lithosphere, *Earth planet. Sci. Lett.,* **133,** 19–34.

Gurnis, M. & Hager, B., 1988. Controls on the structure of subducted slab, *Nature,* **335,** 317–321.

Hager, B.H., 1984. Subducted slabs and the geoid: Constraints on mantle rheology and flow, *J. geophys. Res.,* **89**(B7), 6003–6015.

Hager, B.H., & Richards, M.A., 1989. Long-Wavelength Variations in Earths Geoid—Physical Models and Dynamic Implications, *Phil. Trans. R. Soc. Lond.,* A., **328**(1599), 309–327.

Houseman, G.A. & Gubbins, D., 1997. Deformation of subducted oceanic lithosphere, *Geophys. J. Int.,* **131,** 535–551.

Isacks, B.L. & Barazangi, M., 1977. Geometry of Benioff zone: Lateral segmentation and downwards bending of the subducted lithosphere, *in Deep Sea Trenches and Back-Arc Basins*, pp. 99–114, eds Talwani, M. & Pitman, W.C., Maurice-Ewing Series, Washington D.C.

Jarrard, R.D., 1986. Relations among Subduction Parameters, *Rev. Geophys.,* **24,** 217–284.

Karato, S., Riedel, M.R. & Yuen, D., 2001. Rheological structure and deformation of subducted slabs in the mantle transition zone: Implications for mantle circulation and deep earthquakes, *Phys. Earth planet. Int.,* **127,** 83–108.

Kincaid, C. & Olson, P., 1987. An experimental study of subduction and slab migration, *J. geophys. Res.,* **92,** 13 832–13 840.

King, S.D. & Hager, B.H., 1990. The Relationship between Plate Velocity and Trench Viscosity in Newtonian and Power-Law Subduction Calculations, *Geophys. Res. Lett.,* **17,** 2409–2412.

King, S.D. & Hager, B.H., 1994. Subducted slabs and the geoid: 1. Numerical calculations with temperature-dependent viscosity, *J. geophys. Res.,* **99,** 19 843–19 852.

Lithgow–Bertelloni, C. & Richards, M.A., 1998. The dynamics of Cenozoic and Mesozoic plate motions, *Rev. Geophys.,* **36,** 27–78.

McKenzie, D.P., 1977. The initiation of trenches: A finite amplitude instability, in *Island Arcs Deep Sea Trenches and Back-Arc Basins*, Vol. 1, pp. 57–61, eds Talwani, M. & Pitman, W.C., Maurice-Ewing Series, Washington D.C.

Mitrovica, J.X. & Forte, A.M., 1997. Radial profile of mantle viscosity: Results from the joint inversion of convection and postglacial rebound observables, *J. geophys. Res.,* **102**(B2), 2751–2769.

Molnar, P. & Gray, D., 1979. Subduction of continental lithosphere: some constraints and uncertainties, *Geology,* **7,** 58–62.

Mueller, S. & Phillips, R., 1991. On the initiation of subduction, *J. geophys. Res.,* **96,** 651–665.

Olbertz, D., Wortel, M.J.R. & Hansen, U., 1997. Trench migration and subduction zone geometry, *Geophys. Res. Lett.,* **24,** 221–224.

Pysklywec, R.N. & Mitrovica, J.X., 1998. Mantle flow mechanisms for the large-scale subsidence of continental interiors, *Geology,* **26,** 687–690.

Ranalli, G., 1995. *Rheology of the earth*, 2nd edn, Chapman and Hall, London, p. 413.

Regenauer–Lieb, K. & Branlund, J., 2001. The Initation of Subduction: Criticality by Addition of water?, *Science,* **294,** 578–580.

Richards, M.A. & Engebreston, D.C., 1992. Large-scale mantle convection and history of subduction, *Nature,* **355,** 437–440.

Russo, R.M. & Silver, P.G., 1994. Trench-parallel flow beneath the Nazca plate from seismic anisotropy, *Science,* **263,** 1105–1111.

Shemenda, A.I., 1992. Horizontal lithosphere compression and subduction: constraints provided by physical modeling, *J. geophys. Res.,* **97,** 11 097–11 116.

Tackley, P.J., 2000a. Self-consistent generation of tectonic plates in time-dependent, three-dimensional mantle convection simulations 1. Pseudo-plastic yielding, *G3,* **1**.

Tackley, P.J., 2000b. Self-consistent generation of tectonic plates in time-dependent, three-dimensional mantle convection simulations 2. Strain weakening and astenosphere, *G3,* **1**.

Tao, W.C. & O'Connell, R.J., 1993. Deformation of a weak subducted slab and variation od seismicity with depth, *Nature,* **361,** 626–628.

Tichelaar, B.W. & Ruff, L.J., 1993. Depth of seismic coupling along subduction zones, *J. geophys. Res.,* **98,** 2017–2037.

Turcotte, D.L. & Schubert, G., 1982. *Geodynamics Application of Continuum Physics to Geological Problems*, John Wiley and Sons, New York, p. 450.

Uyeda, S. & Kanamori, H., 1979. Back-arc opening and the mode of subduction, *J. geophys. Res.,* **84,** 1049–1061.

Weijermars, R., 1986. Flow behaviour and physical chemistry of bouncing putties and related polymers in view of tectonic laboratory application, *Tectonophysics,* **124,** 325–358.

Weijermars, R. & Schmeling, H., 1986. Scaling of newtonian and non newtonian fluid dynamics without inertia for quantitative modelling of rock flow due to gravity (including the concept of rheological similarity), *Phys. Earth planet. Int.,* **43,** 316–330.

Yamaoka, K., Fukao, Y. & Kumazawa, M., 1986. Spherical shell tectonics: effects of sphericity and inextensibility on the geometry of the descending lithosphere, *Rev. Geophys.,* **24,** 27–53.

Zhong, S. & Gurnis, M., 1994. Controls on trench topography from dynamic models of subducted slabs, *J. geophys. Res.,* **99,** 15 683–15 695.

Zhong, S. & Gurnis, M., 1995. Towards a realistic simulation of plate margins in mantle convection, *Geophys. Res. Lett.,* **22,** 981–984.

Zhong, S., Gurnis, M. & Moresi, L., 1998. Role of faults, nonlinear rheology, and viscosity structure in generating plates from instantaneous mantle flow models, *J. geophys. Res.,* **103,** 15 255–15 268.